# Wetting Behaviour of Hydrophilic and Hydrophobic Nanostructured Porous Anodic Alumina

*Hannah Leese, Vivek Bhurtun, Kah Peng Lee and Davide Mattia**

Department of Chemical Engineering, University of Bath, Bath, BA27AY, United Kingdom.

Corresponding Author email: d.mattia@bath.ac.uk*, phone: +44 (0)1225-383961

**Abstract**

This paper investigates the effect of surface structure and chemistry on the wetting properties of nanostructured porous anodic alumina (PAA). Measurements of the equilibrium apparent contact angle (APCA) were first taken on as produced hydrophilic nanoporous alumina with a range of pore diameters from 10 to 170 nm, yielding a range of contact angles from 10 to 100°. The PAAs were then coated with a fluorosilane to change the surface chemistry of the nanostructures. The same trend was observed as in the hydrophilic case, but the contact angles increased from 106 to 150° for pores sizes ranging from 10 to 100 nm for the hydrophobic PAA. These results probe the limits of the current wetting models such as the Cassie-Baxter and Wenzel equations for nanostructured materials. A geometric model has been developed using the equation proposed by *Marmur* to explain the wetting properties of the bare- and silanized-PAA.

Keywords: nanostructured alumina; surface chemistry; wetting; contact angle; Wenzel; Cassie-Baxter

## 1. Introduction

The wetting properties of porous materials are traditionally modelled using either the Cassie-Baxter or the Wenzel equations. The former considers a heterogeneous wetting regime, with two or more species with differing contact angles [1]. When the second species is air, the cosine of the apparent contact angle (APCA) can be represented by the following equation:

$$\cos\theta_{CB} = f\left(\cos\theta_Y + 1\right) - 1 \tag{1}$$

where $\theta_{CB}$, is the Cassie-Baxter contact angle, $\theta_Y$ the Young contact angle on a flat smooth surface and *f* the surface fraction of solid wet by the liquid. The latter accounts for the effect of surface roughness on the APCA via a roughness factor, *r*, which constitutes a ratio of the actual surface to its flat smooth projection [2]:

$$\cos\theta_W = r\cos\theta_Y \tag{2}$$

In the first case, the liquid droplet sits above the solid surface and air pockets. In the latter, water penetrates between the crevices of the rough surface. Intermediate cases between these two models can occur, and can be represented by the inhomogeneous wetting regime proposed by Marmur [3]:

$$\cos\theta = r_f f\cos\theta_Y + f - 1 \tag{3}$$

The above equation reduces to Eq. (1) for a non-rough, porous surface $\left(r_f = 1\right)$ and to Eq. 2 (2) for a non-porous, rough surface $\left(f = 1\right)$, when the second species is air.

There has been extensive work to determine a transition between the two regimes [4] and to define a theoretical framework starting from thermodynamic considerations [3, 5, 6]. More recently though, the very validity of both models for surface with nanoscale features has been called into question, with some attributing changes in contact angle to local variations in the line tension due to surface roughness or heterogeneity [7, 8]. Environmental scanning electron microscopy analysis of liquid droplets on high aspect ratio pillar structures has shown the presence of a precursor film which develops at the contact line of the droplet. As a result, the contact line is no longer continuous but breaks down into a distinct set of

interfaces, negating the idea of a macroscopic contact angle [5, 9]. Similarly, contact angle variation has been attributed to the pinning of the contact line rather than the variations in the contact area [10, 11].

Porous anodic alumina (PAA) is a nanostructured material prepared by the electrochemical anodization of aluminium. PAAs are currently used in a variety of areas, ranging from filtration to material templating and as coatings for electronic devices [12-17]. Their attractiveness resides in the possibility of accurately controlling pore size and pore spacing via the anodization parameters, making them an excellent model for systematic studies of material properties at the nanoscale [18]. Wetting of nanoporous alumina by polymers has been used to alter their surface chemistry (i.e. to increase the hydrophobicity) or to fabricate polymer nanotubes [19]. Other studies have modified the surface chemistry and roughness of the alumina systematically by etching the PAA into pillar-like structures and coating with a fluoropolymer to obtain superhydrophobic behaviour (>150°) [20]. In the latter case, a transitional state [21] between Wenzel and Cassie-Baxter was used to explain the observed wetting behaviour, with the pore walls partially wetted by the liquid along with air trapped within the pores. Another recent study also used PAAs to investigate the apparent transition between Wenzel and Cassie-Baxter regimes for pore sizes in the 100-450 nm range [22]. The authors suggest that for the smallest pore sizes investigated, partial wetting of the pore could be observed, whereas for the larger pore diameters the contact angle of the droplet was bigger due to the pores being filled with air. The authors referred to the former case as a 'partial' Wenzel state. Another study looked at the wetting of capped and open PAAs with pore diameters ranging from 40 to 200 nm [23]. Here the authors used the Cassie-Baxter equation, which reported large variations in porosity values with anodization voltage, in contrast with the established notion that porosity values are quasi-constant for PAAs [24, 25]. Interestingly, the two studies above used very different values for the Young's contact angle (the flat, smooth and uniform alumina): 85° in the former [22], and 35° in the latter [23]. Both are very high for alumina, a hydrophilic, high energy solid [26]. A more accepted value for this kind of material is in the order of 10-15° as has been found in previous studies of non-porous alumina [18, 27]. Additionally, the wettability of PAA by different solvents has also been investigated, where four different PAAs with varying pore diameters were analysed (specific diameters values were achieved via etching of

the pores) [18]. The study focused on the interaction between the properties of the liquids (mainly considering the dielectric constant and dipolar moment of the solvents) and the solid surface. It found that DMSO and DMF would fully fill the pores due to the equilibrium between the polar and surface tension properties, whereas water would not fully fill the pores, thus resulting in an increase in contact angle. In all these studies, the Cassie-Baxter and/or the Wenzel equations have been used to model the experimental results obtained. As discussed above, though, the very validity of both models at the nanoscale has been called into question by theoretical studies. In this paper, PAA are used to demonstrate the limitations of both models for wetting by water of nanostructured porous surfaces.

## 2. Experimental Methods

### *2.1 PAA Fabrication*

High purity (99.99%, 10 mm diameter) aluminium discs (Alfa Aesar) were annealed in air at 500 °C for 60 minutes, degreased in acetone, and subsequently electropolished (1:4 v/v $HClO_4$/EtOH) prior to the first step of anodization. The pristine substrates were then anodized at 10 – 25 V and 30 – 80 V in 0.5 M sulfuric acid ($H_2SO_4$) and 0.3 M oxalic acid ($H_2C_2O_4$) electrolytes, respectively, for 20 minutes (see Table S1 in the supplementary information for details on anodization). The alumina formed from the first step was subsequently removed by wet chemical etching using a 1:1 mixture of 6 wt% $H_3PO_4$ and 1.8 wt% $H_2CrO_4$ at 60 °C for 15 minutes [18]. Immediately after the oxide removal the substrate was anodized again (with the same conditions as in the first step) for 5-6 hours for the sulfuric and 10-12 hours for the oxalic electrolyte, respectively. PAAs were also silanized using a simple process developed by Aran *et al.* [28]. Briefly, 40 µl of fluorooctyltrichlorosilane (FOTS) were dropped into 40 ml of n-hexane. Each PAA sample was then placed inside the FOTS-hexane solution for 1 hour with gentle agitation. The PAAs were then taken out of the solution, rinsed and placed in an oven at 100 °C for 1 hour. The samples were then rinsed with acetone and left to dry.

*2.2 Characterization of PAA*

The pore diameter $(D_p)$, interpore spacing $(D_c)$, barrier layer thickness $(B)$ and porosity $(p)$ were each measured via statistical image analysis of SEM micrographs and atomic force microscopy (AFM) images. A Carl Zeiss XB1540 Gemini® FESEM microscope and AFM Veeco Multimode with Nanoscope III controller were used in this work. The images were also subsequently analyzed with ImageJ and Gwyddion Software packages. Membrane thickness $(L)$ was measured using a micrometer with ± 5 μm accuracy.

Contact angle measurements were made using the sessile droplet method in air at room temperature with 5 μ$L$ droplets of di-ionized (DI) water as the solvent. The alumina substrate was washed with DI water and HPLC grade ethanol and then thoroughly dried with an Argon stream. The alumina substrate was then placed on the goniometer and still images were obtained using a Discovery VMS-001 USB microscope (Veho). The subsequent images were used to calculate the contact angle of the droplet, utilizing Dropsnake software with the ImageJ imaging process package [18]. Each data point is an average of 6 measurements within the error ± 2°.

SEM micrographs of the porous structure are shown in Fig. 1 (a)-(c). A regular pore structure was observed for all samples, with limited branching only observed in the sample with the smallest average pore diameter (Fig. 1 (a)). Cross-sections of the membranes were obtained via focused ion beam sectioning, confirming the regularity of the pore structure along the membrane thickness and confirming the pore channels were capped at one end (Fig. 1 (e)). From the results obtained using the SEM and AFM micrographs the average pore diameter and porosity have been related to the anodization voltage. The proportionality constant between average pore diameter and anodization voltage (1.25 nm $V^{-1}$) supports previous findings [24]. The porosity varies in the 10-20% range for all membranes, as reported in literature [24]. Numerical values of all quantities measured are reported in Table S1.

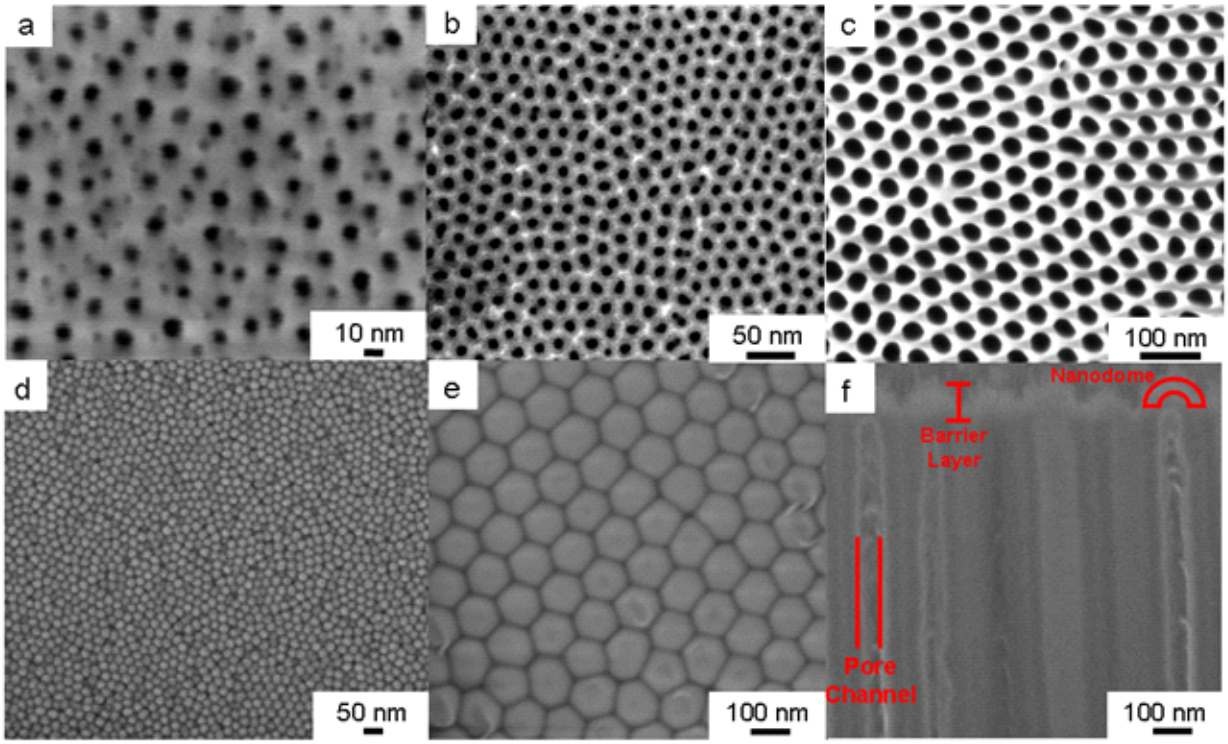


**Fig. 1.** FE-SEM image of ordered PAAs top surface (a) average $D_p$ = 13 nm (10 V, 0.5 M sulfuric, 0°C); (b) average $D_p$ =30 nm (25 V, 0.5 M sulfuric, 0°C); (c) average $D_p$ = 44 nm (40 V, 0.3 M oxalic, 14°C); (d-e) FE-SEM of capped PAAs bottom surface; (f) Cross section of PAA and barrier oxide layer.

### 3. Results and Discussion

The equilibrium APCA of water on the PAAs increases linearly with pore diameter in the range investigated (10-100 nm) up to approximately 100° for the bare alumina and 150° for the silanized case (Fig. 2). Extrapolation of the contact angle data for $D_p = 0$, i.e. for a solid smooth surface yields a contact angle of ~13° and ~103° for bare-PAA and silanized-PAA, respectively. The extrapolated values are in good agreement with previously published data [27] and contact angle measurements performed on a slab of bare (12±2°) and silanized (103±2°) alumina. From data in Fig. 2, it can be seen that the contact

angle increases linearly with the pore diameter until a critical value, $D_p^*$ , after which the contact angle increase slows down, more markedly for the silanized surfaces than for the bare PAAs.

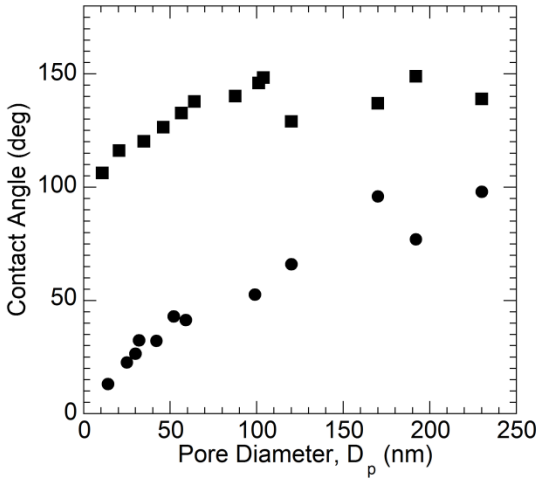


**Fig. 2.** Water APCA on bare-PAA (●) and silanized-PAA (■) as a function of the average pore diameter, (error ±2°).

For $D_p < D_p^*$, both curves in Fig. 2 have the same slope ~0.4° nm$^{-1}$, yielding the following relationship between the cosine of the APCA and pore diameter:

$$\cos\theta_{\exp}^{i} = \alpha^{i}\theta_{Y}^{i} + \kappa^{i}D_{p} \tag{4}$$

where $\theta_{exp}$ is the experimental contact angle, $\theta_Y$ the Young's contact angle (CA) on a flat surface (i.e. flat alumina), α and κ are derived experimentally and $i$ = bare- or silanized-PAA. The equation shows that the contribution to the contact angle of the surface structure can be decoupled from the surface chemistry contribution, given by the Young contact angle for the bare and silanized surfaces. The surface chemistry represents a constant contribution to the contact angle whereas the changing pore diameters result in a variable contribution to the contact angle i.e. the smaller the structure the closer the contact angle is to the Young's contact angle. The combination of both of these factors ultimately increases the contact angle of both the hydrophilic and the hydrophobic nanostructures. For $D_p > D_p^*$, it appears that the APCA for the

silanized surfaces becomes constant around or just below 150°. For the bare surface, after crossing the 90° threshold, the contact angle increase is slowed down compared to the first segment.

As the APCA increases with increasing pore diameter, the Cassie-Baxter equation for a porous, non-rough surface appears to be the obvious choice to model the experimental data. The porosity alone, though, is not sufficient to explain the increase in contact angle, as will be discussed later. This can be attributed to the well-known characteristic of PAAs to have a quasi-constant porosity of approximately 10-20% [24]. This is due to the fact that as the pore size increases, the number of pores decreases exponentially, leaving the porosity to be quasi-independent from anodization voltage. The limits associated with the term $f$ in the Cassie-Baxter equation have been addressed in detail elsewhere [5]. Several adapted Cassie-Baxter models have been developed, but all still depend on the solid surface fraction varying when the structures size increases [7, 29].

If the porosity alone is not responsible for the increase in contact angle, then this has to be associated with a larger interaction of the liquid with the solid, i.e. some penetration of the liquid inside the pore has to occur. This phenomenon has been observed for both hydrophilic and hydrophobic porous surfaces [4]. The extent of penetration is given by a balance of the Laplace pressure of the macroscopic liquid drop on the substrate surface $\left(\frac{2\gamma_{LV}}{r}\right)$ [9, 30] and the resistance to compression of the air in the pores (assuming that it behaves as an ideal gas and that no air escapes from the pores):

$$p_1 V_1 = p_2 V_2 \tag{5}$$

where $p_1 = p_{atm}$ and,

$$V_1 = \frac{\pi D_p^2 L}{4} \tag{6}$$

When the liquid is partially filling the pore (Fig. 3), then

$$p_2 = p_1 + \frac{2\gamma_{LV}\cos\theta}{r} \text{ and } V_2 = \frac{\pi D_p^2 (L-\delta)}{4} \quad (7)$$

where $\delta$ is the pore filling depth (i.e. how deep the droplet goes into the pore – full penetration would yield $\delta = L$). All other symbols are described in Fig. 3a. For simplicity, this model considers the bottom of the pore to be flat (see Fig. S1); however in reality it has the shape of a spherical cap of radius $D_p / 2$ (due to the barrier oxide layer). Given that $\frac{L}{D_p} > 10^3$, the error associated with this is in the order of 0.1%. The Laplace pressure exercised by the droplet is significantly different for the two surfaces, given the different wetting properties (Fig. 3b). In fact, it somewhat mirrors the APCA behaviour shown in Fig. 2. It is noted here that since the drop diameter for the lowest contact angles in the bare alumina case is larger than the capillary number for water, the height of the liquid films was used in lieu of the radius to calculate the Laplace pressure [4].

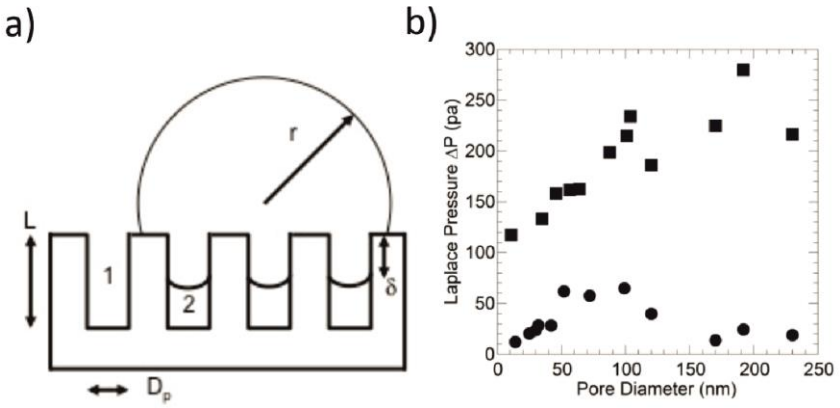


**Fig. 3.** (a) Schematic of water droplet penetration inside cylindrical channels of length *L* and diameter $D_p$ for a silanized, hydrophobic, PAA. The liquid penetrates inside the pores by a depth $\delta \le L$, as a function of water drop diameter, $r$ and pressure of air trapped inside the pore. (b) Laplace pressure of water droplets on silanized (■) and bare (●) PAAs as a function of pore diameter.

For $D_p < D_p^*$, the dependency of cosine of the APCA on the pore diameter can be modelled using the inhomogeneous wetting regime (Eq. (3)). Comparing Eq. (3) and (4), one obtains that:

$$f = 1 - \kappa D_p \tag{8}$$

$$r_f = \frac{\alpha}{1 - \kappa D_p} \tag{9}$$

As $r_f$ is defined as the ratio between the actual wet surface and its smooth projection, in the case of the PAAs it is defined as [3]:

$$r_f = 1 + \frac{4p\delta}{(1-p)D_p} \tag{10}$$

where the porosity $p = \frac{\sum_{i=1}^{n} \pi D_p^2 / 4}{A_S} \cong \frac{n\pi D_p^2}{4A_S}$ . Here $n$ is the number of pores and $A_S$ the drop-solid contact surface for each value of $D_p$ . The second relation is only valid when the pore size distribution is narrow, as is the case for the PAAs used here [18]. This expression for $r_f$ results in an excellent agreement with experimental data, for $D_p < D_p^*$ (Fig. 4).

As can be observed from Fig. 4, $f$ decreases with increasing pore diameter, ideally down to 0 when $D_p = 1/\kappa$, where $\kappa$ is obtained experimentally from Eq. (3). The fact that $f$ decreases might appear to be in contradiction with the experimental evidence that pore filling increases with increasing pore diameter. In reality, the effect of the reduction of the drop-solid surface has to be taken into account and this is significantly larger than the increase given by the liquid filling the pore. As such, *f* can be defined as:

$$f = (1-p)\frac{A_S}{A_0} \tag{11}$$

where $A_0$ is the droplet area on a flat, smooth surface where $\theta = \theta_Y$. When $\delta = 0$, $r_f = 1$ and $f = 1$, it corresponds to a flat, smooth surface, $A_S = A_0$. On the other hand, when $D_p = 1/\kappa$, then $f \sim 10^{-8} \simeq 0$, as the macroscopic droplet size would ideally coincide with a single pore diameter, with no liquid in contact with the PAA surface except for the (small) portion of pore wall wet by the liquid. This case, though, is never reached as can be seen in Fig. 4, where the values for $r_f$ and $f$ obtained using Eq. (10) and (11) deviate from experimental data. The reason for this behaviour is discussed below. The inflection point corresponds with $D_p = D_p^*$, as in Fig. 2.

The behaviour for $D_p > D_p^*$ is discussed below separately for the silanized- and bare-PAAs.

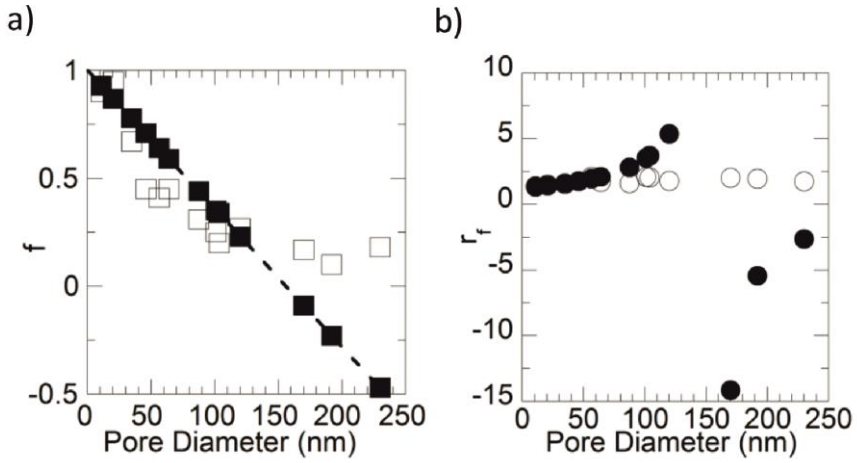


**Fig. 4.** (a) parameter (■) $f = 1 - \kappa D_p$ and (□) $f = (1-p)\frac{A_S}{A_0}$; (b) (●) $r_f = \frac{\alpha}{1-\kappa D_p}$ and (○) $r_f 1 + \frac{4p\delta}{(1-p)D_p}$ for silanized PAAs as a function of pore diameter. The behaviour is similar for the bare PAAs.

By substituting the expressions for $r_f$ and $f$ in Marmur's model [3], a good correlation with experimental data is obtained (Fig. 5, with the Cassie-Baxter and Wenzel equations for the silanized PAAs drawn in bold dashed lines).

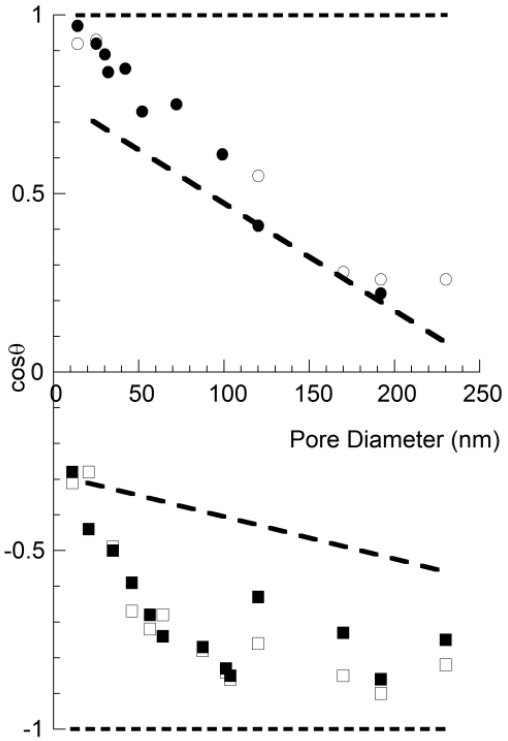


**Fig. 5.** Cosine of the APCA for experimental data (■), (●) and model data (□), (○) data for the silanized and bare PAAs derived from Eq. (3), respectively. The Cassie-Baxter and Wenzel models are shown as dashed lines, based on Eq. (1) and (2), respectively.

*3.1 Wetting of (hydrophobic) Silanized PAAs*

For the silanized PAAs, the Laplace pressure first increases linearly starting from a value as low as 32 Pa followed by a quasi-constant value around 100 Pa. Previous experiments in the literature have shown that pressure can induce a wetting transition from a Cassie-Baxter to a Wenzel-type behaviour [4, 9]. It is quite clear that for the smallest pores, there is little to no penetration of the liquid inside the pores of silanized PAAs, consistent with Cassie-Baxter behaviour. In fact, the Laplace pressure of the water droplet formed for the case of the PAA with the smallest pore size is below the 50-100 Pa threshold for inducing penetration, as reported in the literature [4, 9]. As the APCA increases, the Laplace pressure increases and penetration of water inside the pores occurs, leading to a Wenzel-like behaviour. Above $D_p^*$, though, the cosine of the APCA is about -0.8, somewhat short of the -1 value that one would obtain

if the whole pore were to be filled with water in an ideal Wenzel behaviour. This is attributed to the fact that the pore is not completely filled and the pore filling depth, $\delta$, is a function not only of the PAA geometric characteristics, pore diameter and pore length, but also of the Laplace pressure of the overlaying droplet. A full Wenzel case $\left(\delta \equiv L, r_f \equiv r \gg 1\right)$ could indeed be achieved by applying further external pressure, as shown in the literature [4]. It should be noted that this could occur only if all the air present in the pores were to be replaced by water. While some evolution of air bubbles out of hydrophilic PAA pores through a liquid droplet has been observed before [22], the same behaviour appears unrealistic for a hydrophobic surface.

*3.2 Wetting of (hydrophilic) Bare PAAs*

As can be seen in Fig. 2, the contact angle increase for the bare case is more linear than that for the silanized PAAs. It could also be argued that it is fully linear and no slow-down is observed, within the margin of error of experimental data. The shape of the Laplace pressure curve points in the latter direction within experimental error, though the overall value of the pressure is much lower, just at or below the threshold for liquid penetration for hydrophilic surfaces reported in the literature [9]. It should be noted, however, that since the bare PAAs are very hydrophilic, there is a strong capillary pressure for the liquid to enter the pore, and none are withstanding the resistance of the air trapped in the pores. The rationale for the APCA change with pore diameter is opposite to that of the silanized substrates: The pores are initially penetrated by water and, as the pore size increases, more and more air is trapped in the pores leading to a higher contact angle. As discussed in the introduction, a previous study has looked at the wetting behaviour of bare PAAs with pores in the 100-450 nm range [22], with a wetting transition from the Wenzel to Cassie-Baxter regime above 250 nm. This was justified, in particular, by assuming the Young contact angle for alumina to be $\theta_Y$ =85°. This is a high value for alumina, a high energy solid [26]. In addition, as suggested earlier, literature data of the contact angle of water on alumina is more closely aligned with the 10-12° value reported here. The experimental results from [22] have been combined with

the ones reported in this paper (Fig. 6, ○ and ●, respectively) showing good agreement in a linear correlation between the contact angle and the pore diameter. These results lead to challenging the model proposed in [22], as the transition between the Wenzel and Cassie-Baxter regimes starts for much smaller pores than what has been previously analysed. The results can be explained assuming the inhomogeneous wetting regime in Eq. (3) with the parameters in Eq. (10) and (11).

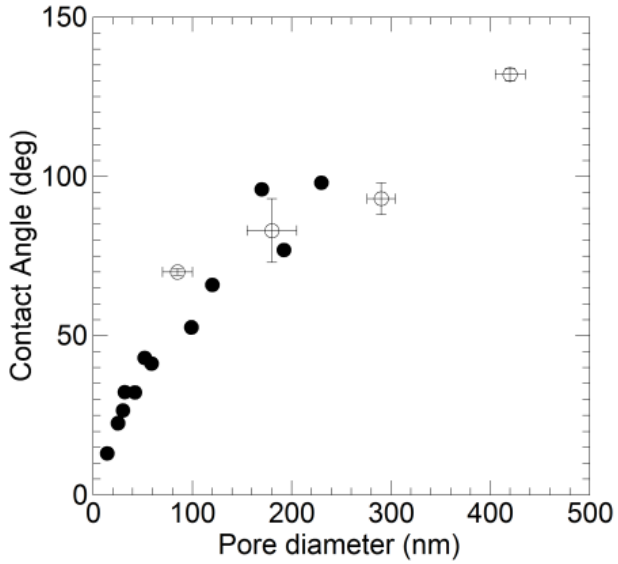


**Fig. 6.** Comparison of contact angle values for water on bare, hydrophilic PAAs: this study (●, error ± 2°), and (○, error bars from paper) Ran *et. al.* [22].

Finally, it is noted here that the linear variation of contact angle with increasing pore diameter (and anodization voltage) in Fig. 3 is conserved when passing from samples anodized in sulfuric, in oxalic and in phosphoric acid (Table S1). While it is well-known that anions from the electrolytes are incorporated in the alumina during the anodization process [24], no significant differences in contact angle due to the presence of anions are expected, since they will not significantly alter the charge state of the alumina surface [27, 31]

## 4. Conclusions

This study has systematically tested the wetting properties of nanoscale pore bare- and silanized- PAAs. By varying the anodization parameters the wettability of the bare-PAA was changed, thereby yielding APCA from 10° to 100°, which were dependent on the pore diameter, but not on the porosity, highlighting a limit of the Cassie-Baxter equation in modelling porous nanostructures with constant porosity values for increasing pore size. The surface chemistry of the PAA samples was modified using FOTS to investigate the effect of surface chemistry and structure of the PAA on the APCA and further support the findings that in this particular case the Cassie-Baxter and Wenzel equations do not model the experimental findings. The comparison of the wetting behaviour of the two surfaces allowed the contributions to wetting given by the surface nanostructure and chemistry to be separated. The inhomogeneous regime was successfully adapted to model the experimental data with analytical expressions for the two model parameters, even for the smallest pore sizes, without the need to use the line tension to fit the experimental data.

## Acknowledgements

The authors acknowledge the UK EPSRC (grant EP/G045798/1) and the EU (grant PIRG03-GA-2008-230876) for funding support. This work was also supported by the NanoAccess in Cardiff, EPSRC [EP/F056745/1]. The contents reflect only the authors' views and not the views of the European Commission.

## References

[1] A.B.D. Cassie, S. Baxter, Wettability of Porous Surfaces, T. Faraday Soc. 40 (1944) 546-551.

[2] T.N. Wenzel, Surface Roughness and Contact Angle, J. Phys. Chem. 53 (1949) 1466.

[3] A. Marmur, Wetting on Hydrophobic Rough Surfaces: To Be Heterogeneous or Not To Be?, Langmuir 19 (2003) 8343-8348.

[4] A. Lafuma, D. Quere, Superhydrophobic states, Nat. Mater. 2 (2003) 457-460.

[5] E. Bormashenko, Why does the Cassie-Baxter equation apply?, Colloid Surface. A. 324 (2008) 47-50.

[6] G.O. Berim, E. Ruckenstein, Microscopic Interpretation of the Dependence of the Contact Angle on Roughness, Langmuir 21 (2005) 7743-7751.

[7] Y. Kwon, S. Choi, N. Anantharaju, J. Lee, M.V. Panchagnula, N.A. Patankar, Is the Cassie−Baxter Formula Relevant?, Langmuir 26 (2010) 17528-17531.

[8] E. Bormashenko, A Variational Approach to Wetting of Composite Surfaces: Is Wetting of Composite Surfaces a One-Dimensional or Two-Dimensional Phenomenon?, Langmuir 25 (2009) 10451-10454.

[9] E. Bormashenko, Y. Bormashenko, T. Stein, G. Whyman, R. Pogreb, Z. Barkay, Environmental Scanning Electron Microscopy Study of the Fine Structure of the Triple Line and Cassie−Wenzel Wetting Transition for Sessile Drops Deposited on Rough Polymer Substrates, Langmuir 23 (2007) 4378-4382.

[10] L.C. Gao, T.J. McCarthy, How Wenzel and Cassie Were Wrong, Langmuir 23 (2007) 3762-3765.

[11] J. Liu, Y. Mei, R. Xia, A New Wetting Mechanism Based upon Triple Contact Line Pinning, Langmuir 27 (2010) 196-200.

[12] C.R. Martin, Nanomaterials: A Membrane-Based Synthetic Approach, Science 266 (1994) 1961-1966.

[13] G.E. Thompson, Porous anodic alumina: fabrication, characterization and applications, Thin Solid Films 297 (1997) 192-201.

[14] G. Che, B.B. Lakshmi, C.R. Martin, E.R. Fisher, Chemical Vapor Deposition Based Synthesis of Carbon Nanotubes and Nanofibers Using a Template Method, Chem. Mater. 10 (1998) 260-267.

[15] H. Orikasa, N. Inokuma, S. Okubo, O. Kitakami, T. Kyotani, Template Synthesis of Water-Dispersible Carbon Nano "Test Tubes" without Any Post-treatment, Chem. Mater. 18 (2006) 1036-1040.

[16] Y. Yang, H. Chen, Y. Mei, J. Chen, X. Wu, X. Bao, Anodic alumina template on Au/Si substrate and preparation of CdS nanowires, Solid State Commun. 123 (2002) 279-282.

[17] M. Gowtham, L. Eude, C.S. Cojocaru, B. Marquardt, H.J. Jeong, P. Legagneux, K.K. Song, D. Pribat, Controlled fabrication of patterned lateral porous alumina membranes, Nanotechnology 19 (2008) 035303.

[18] K.P. Lee, H. Leese, D. Mattia, Water flow enhancement in hydrophilic nanochannels, Nanoscale 4 (2012) 2621-2627.

[19] M. Steinhart, J.H. Wendorff, A. Greiner, R.B. Wehrspohn, K. Nielsch, J. Schilling, J. Choi, U. Gösele, Polymer Nanotubes by Wetting of Ordered Porous Templates, Science 296 (2002) 1997.

[20] W. Lee, B.G. Park, D.H. Kim, D.J. Ahn, Y. Park, S.H. Lee, K.B. Lee, Nanostructure-Dependent Water-Droplet Adhesiveness Change in Superhydrophobic Anodic Aluminum Oxide Surfaces: From Highly Adhesive to Self-Cleanable, Langmuir 26 (2010) 1412-1415.

[21] S. Wang, L. Jiang, Definition of Superhydrophobic States, Adv. Mater. 19 (2007) 3423-3424.

[22] C. Ran, G. Ding, W. Liu, Y. Deng, W. Hou, Wetting on Nanoporous Alumina Surface: Transition between Wenzel and Cassie States Controlled by Surface Structure, Langmuir 24 (2008) 9952-9955.

[23] Z.R. Li, J.X. Wang, Y.Z. Zhang, J.J. Wang, L. Jiang, Y.L. Song, Closed-air induced composite wetting on hydrophilic ordered nanporous anodic alumina, Appl. Phys. Lett. 97 (2010) 233107.

[24] G.D. Sulka, Highly ordered anodic porous alumina formation by self-organized anodizing, in: A. Eftekhari (Ed.) Nanostructured Materials in Electrochemistry, Wiley-VCH, Weinheim, 2008.

[25] K. Nielsch, J. Choi, K. Schwirn, R.B. Wehrspohn, U. Gosele, Self-ordering Regimes of Porous Alumina: The 10 Porosity Rule, Nano Lett 2 (2002) 677-680.

[26] P.G. de Gennes, F. Brochard-Wyard, D. Quere, Capillarity and wetting phenomena: drops, bubbles, pearls, waves, Springer, New York, 2004.

[27] D. Megias-Alguacil, E. Tervoort, C. Cattin, L.J. Gauckler, Contact angle and adsorption behavior of carboxylic acids on $\alpha$-$Al_2O_3$ surfaces, J. Colloid Interf. Sci. 353 (2011) 512-518.

[28] H.C. Aran, J.K. Chinthaginjala, R. Groote, T. Roelofs, L. Lefferts, M. Wessling, R.G.H. Lammertink, Porous ceramic mesoreactors: A new approach for gas–liquid contacting in multiphase microreaction technology, Chem. Eng. J. 169 (2011) 239-246.

[29] S.T. Larsen, R. Taboryski, A Cassie-Like Law Using Triple Phase Boundary Line Fractions for Faceted Droplets on Chemically Heterogeneous Surfaces, Langmuir 25 (2009) 1282-1284.

[30] V. Raspal, K.O. Awitor, C. Massard, E. Feschet-Chassot, R.S.P. Bokalawela, M.B. Johnson, Nanoporous Surface Wetting Behavior: The Line Tension Influence, Langmuir 28 (2012) 11064-11071.

[31] G.V. Franks, L. Meagher, The isoelectric points of sapphire crystals and alpha-alumina powder, Colloid Surface. A. 214 (2003) 99-110.